Inelastic scattering of protons, ^{3}He, and ^{4}He at 30 MeV/nucleon from ^{166}Er and ^{176}Yb and quadrupole moments of the optical potential

O. Kamigaito,* H. Sakaguchi, M. Nakamura, S. Hirata,* H. Togawa,* T. Nakano,†
M. Yosoi, M. Ieiri,‡ T. Ichihara,§ H. M. Shimizu, Y. Nakai, and S. Kobayashi
Department of Physics, Kyoto University, Kyoto 606, Japan
(Received 11 November 1991)

Elastic and inelastic scattering of polarized protons, ^{3}He particles, and ^{4}He particles from ^{166}Er and ^{176}Yb have been measured at the incident energy of 30 MeV/nucleon. Coupled-channels analyses have been performed using the deformed optical potentials (DOP's) based on the symmetric rotational model. The quadrupole (Q_2) moments of the real parts of the DOP's for the ^{4}He scattering have been found to be larger than those of the charge distributions by about 5%. They are well explained by the folding model calculation with the density-dependent M3Y interaction. The Q_2 moments for the proton and the ^{3}He scattering are almost equal to or smaller than the charge quadrupole moments, and are not reproduced by the conventional folding model. These discrepancies suggest that there are other important reaction mechanisms not being explained in terms of the folding model with the effective interaction. For the proton scattering, the explicit coupled-channels calculations including neutron pickup channels are found to reduce largely the discrepancies in the Q_2 moments. Breakup channels are expected to give a significant contribution to the small Q_2 moments of the DOP's for the ^{3}He scattering.

PACS number(s): 25.40.Ep, 25.55.Ci, 24.10.Ht

I. INTRODUCTION

Intensive study of the 65-MeV proton inelastic scattering from lanthanide and actinide nuclei has shown that the multipole moment of deformed optical potentials (DOP's) is a powerful tool to investigate nuclear reaction mechanisms from a microscopic point of view [1–3]. These scattering data have been well reproduced by the coupled-channels analyses using the DOP's and the multipole moments have been determined precisely. It has been found that the quadrupole (Q_2) moments of the real part of the DOP's are larger than those of the charge distributions and that their values are well explained in terms of the density dependence of the effective interaction, which arises from many-body effects of the nucleon-nucleon interaction in nuclei.

In considering the density dependence of the effective interaction from the multipole moments, folding models play an important role. If one obtains a deformed optical potential $U(\mathbf{r})$ by folding a density-independent interaction $V(r)$ over a matter distribution $\rho_A(\mathbf{r})$ of a deformed nucleus,

$$U(\mathbf{r})=\int \rho_A(\mathbf{r}_A)V(|\mathbf{r}-\mathbf{r}_1|)d\mathbf{r}_A \ , \tag{1}$$

the multipole moments of the folded potential and those of the matter distribution are equal to each other [4]:

$$Q_\lambda(U)=Q_\lambda(\rho_A) \ , \tag{2}$$

where the multipole moment of a function $f(\mathbf{r})$ is defined as follows:

$$Q_\lambda(f)=\frac{\int f(\mathbf{r})r^\lambda Y_{\lambda 0}(\theta)d\mathbf{r}}{\int f(\mathbf{r})d\mathbf{r}} \ . \tag{3}$$

The nucleon-nucleon interaction in nuclei is, however, expressed in a density-dependent form involving many-body properties of the interaction, and the multipole moments of the DOP's are not always the same as those of the matter distributions. Thus, the differences between the multipole moments of the DOP's and those of the matter distributions reflect the density dependence of the effective interaction, or the many-body effects of the nucleon-nucleon interaction in nuclei.

It is important to note that Eqs. (1) and (2) hold without any limitation on the interaction range. This means that we can discuss the density dependence free from the range of the effective interaction. Furthermore, from their definition, the multipole moments of the DOP's are sensitive to the nuclear surface region where most of the nuclear reactions take place.

It has been shown from the ^{166,168}Er(p,p') and the ^{174,176}Yb(p,p') reactions at $E_p=65$ MeV that the Q_2 moments of the real parts of the DOP's are 4–6 % larger than those of the charge distributions [1]. The Q_2 moments for Hf, W, U, and Th isotopes were found to be 2–4 % larger than those of the charge distributions [2,3]. These large Q_2 moments of the DOP's are mainly attri-

*Present address: Research Center for Nuclear Physics, Osaka University, Ibaraki, Osaka 567, Japan.
†Present address: Department of Physics, University of Alberta, Edmonton, Canada T6G 2N5.
‡Present address: National Laboratory for High Energy Physics, Ibaraki 305, Japan.
§Present address: The Institute of Physical and Chemical Research (RIKEN), Wako, Saitama 351, Japan.

buted to the Pauli-blocking effect involved in the density dependence of the effective interaction. Since this effect reduces the interaction strength when the density of nucleons is high, the Q_2 moment of the folded potential becomes larger than that of the matter distribution. In fact, the Q_2 moments of the DOP's for these reactions have been well reproduced by the folding model calculations [1–3] based on the DDM3Y (density-dependent M3Y) [5] and the CEG (complex effective Gaussian) interaction [6], assuming the multipole moments of the neutron density equal to those of the proton density [7].

In contrast to the excellent explanation of the folding model for the Q_2 moments for the 65-MeV protons, it has been pointed out recently that the Q_2 moments of the real parts of the DOP's for the ^{166,168}Er(d,d') and ^{174,176}Yb(d,d') reactions at $E_d=56$ MeV are smaller than, or nearly equal to, those of the charge distributions [8]. The Q_2 moments for the 56-MeV deuteron scattering from Sm isotopes are also nearly equal to those of the charge distributions [9]. These Q_2 moments cannot be explained by the folding model calculation because, as mentioned above, the folding calculation provides the Q_2 moments larger than those of the matter distributions. There are two possibilities to explain the discrepancy between the Q_2 moments of the DOP's for the 56-MeV deuterons and those of the folded potentials [8]. One is that this is due to the effect of the breakup channels of incident deuterons, which is not treated within the framework of the folding model. Although there exists no explicit calculation including the breakup channels for these reactions, this contribution is expected to be significant in the case of the deuteron scattering [10]. The other explanation is that the energy dependence of the effective interaction may not be correctly treated at the 30-MeV/nucleon region. It is, however, hard to draw such a conclusion from the experiment of deuterons where the effect of the breakup channels is not negligible. Therefore, these two explanations would be only qualitative ones.

Inelastic scattering of other light ions at the 30-MeV/nucleon region from the deformed nuclei is expected to provide more valuable information for the microscopic study of the nuclear reaction mechanisms through the multipole moments of the DOP's. These multipole moments can be determined precisely because these nuclei have stable and static deformation, and the excitations of the rotational levels are well described by the coupled-channels analyses based on the DOP's. In this work, we measured elastic and inelastic scattering of polarized protons, ^{3}He particles, and ^{4}He particles at the incident energy of 30 MeV/nucleon from ^{166}Er and ^{176}Yb. Since the measurements were performed at the same incident energy per nucleon, the ambiguities arising from the energy dependence of the effective interaction can be eliminated in comparing the Q_2 moments of the DOP's for the different projectiles with each other. The inelastic scattering of the composite projectiles will give us a criterion for the effect of the breakup channels on the DOP's. ^{3}He particles are, like deuterons, weakly bound particles and the effect would be more significant on the DOP's for the ^{3}He particles than those for the ^{4}He particles. For the proton scattering, discussions can be done free from the breakup channels.

II. EXPERIMENTAL PROCEDURE AND DATA REDUCTION

The experiment has been carried out using 30-MeV polarized protons, 90-MeV ^{3}He particles, and 120-MeV ^{4}He particles from the AVF Cyclotron at RCNP, Osaka University. The data have been obtained using the high-resolution spectrograph RAIDEN [11].

The polarized proton beam was obtained by the atomic-beam-type polarized ion source [12] whose details are described in our previous paper [1]. The beam polarization was monitored with the sampling-type polarimeter [13] during the experiment. A polyethylene analyzer target of the polarimeter was placed in the beam line for a few seconds to measure the beam polarization with an interval of 10–40 sec. The measurements of the position spectra were performed only when the polarimeter was out of the beam in order to avoid any deterioration of the beam quality due to the polarimeter target. The spin orientation of the incoming protons was reversed every 0.5 sec in order to reduce the instrumental asymmetry. The typical beam polarization was 80% and the typical intensity was 20 nA on the target. The ^{3}He beam and the ^{4}He beam were obtained from the internal ion source. The typical intensities on the target were 250 nA for the ^{3}He beam and 140 nA for the ^{4}He beam. The beam intensities were adjusted to keep a proper counting rate ($\leq$600 cps).

The scattered particles were detected by a counter array [14] at the focal plane, which consists of a two-dimensional position-sensitive proportional counter (1.5 m length), a dual single-wire proportional counter (ΔE counter), and a plastic scintillator (E counter). A pileup rejector was employed to reduce the background in the position spectra. Event triggers were generated by the signals from the plastic scintillator. All the signals from the counter system were digitized by analog-to-digital convertors and transferred to a PDP11/44 computer through the raw data processor [15]. All the data were recorded on magnetic tapes in the list mode. The event trigger signals were also counted by a 100-MHz scalar to correct the counting losses of the data-taking system.

The targets are self-supported enriched metal foils. The enrichment of ^{166}Er and ^{176}Yb in the foils are 97.69 and 96.68 %, respectively. The foil thickness is 1.0 and 2.0 mg/cm^2 for Er, and 2.0 mg/cm^2 for Yb. The foil of 1.0 mg/cm^2 was used for the measurement of the ^{4}He scattering at the forward angles ($10°\leq\theta_{\rm lab}\leq 35°$). The efficiency of the position counter was checked along the focal plane, by measuring the elastic scattering with various $B\rho$ values. The efficiency was uniform within the deviation of 1%. For the measurement of the proton scattering, the solid angles were set to be 1.36 msr at the forward angles ($10°\leq\theta_{\rm lab}\leq 35°$) and 2.5 msr at the backward angles ($35°\leq\theta_{\rm lab}\leq 95°$). The current integration has been checked by measuring the elastic scattering from ^{27}Al at $\theta_{\rm lab}=50°$, where the cross section is known [16].

For the measurement of the ^{3}He and the ^{4}He scattering, the solid angles were set to be 0.336 msr at the forward angles ($10° \leq \theta_{lab} \leq 30°$), 0.840 msr at the medium angles ($30° \leq \theta_{lab} \leq 50°$), and 1.279 msr at the backward angles ($50° \leq \theta_{lab} \leq 62°$).

The position spectra at the focal plane were constructed employing particle identification gates using the signals of the ΔE counter. The overall dead-time corrections have been carried out for the position spectra. Figure 1 shows typical position spectra. We have evaluated the peak areas of the 0^+ and the 2^+ states by use of the peak-fitting code developed in our previous work [2]. The χ^2 values per data point in this peak-fitting procedure were 1.0–2.5. The statistical uncertainties of the peak sums were calculated by solving the error matrices.

The experimental cross sections and the analyzing powers are plotted in Figs. 2–7. The error bars on the experimental data represent only the statistical uncertainties.

III. ANALYSIS

Coupled-channels analyses [17] have been performed for three or four members of the ground-state rotational band using the automatic search code ECIS by Raynal [18]. It was assumed that these states are members of a $K^\pi = 0^+$ rotational band of the axially symmetric rigid rotor.

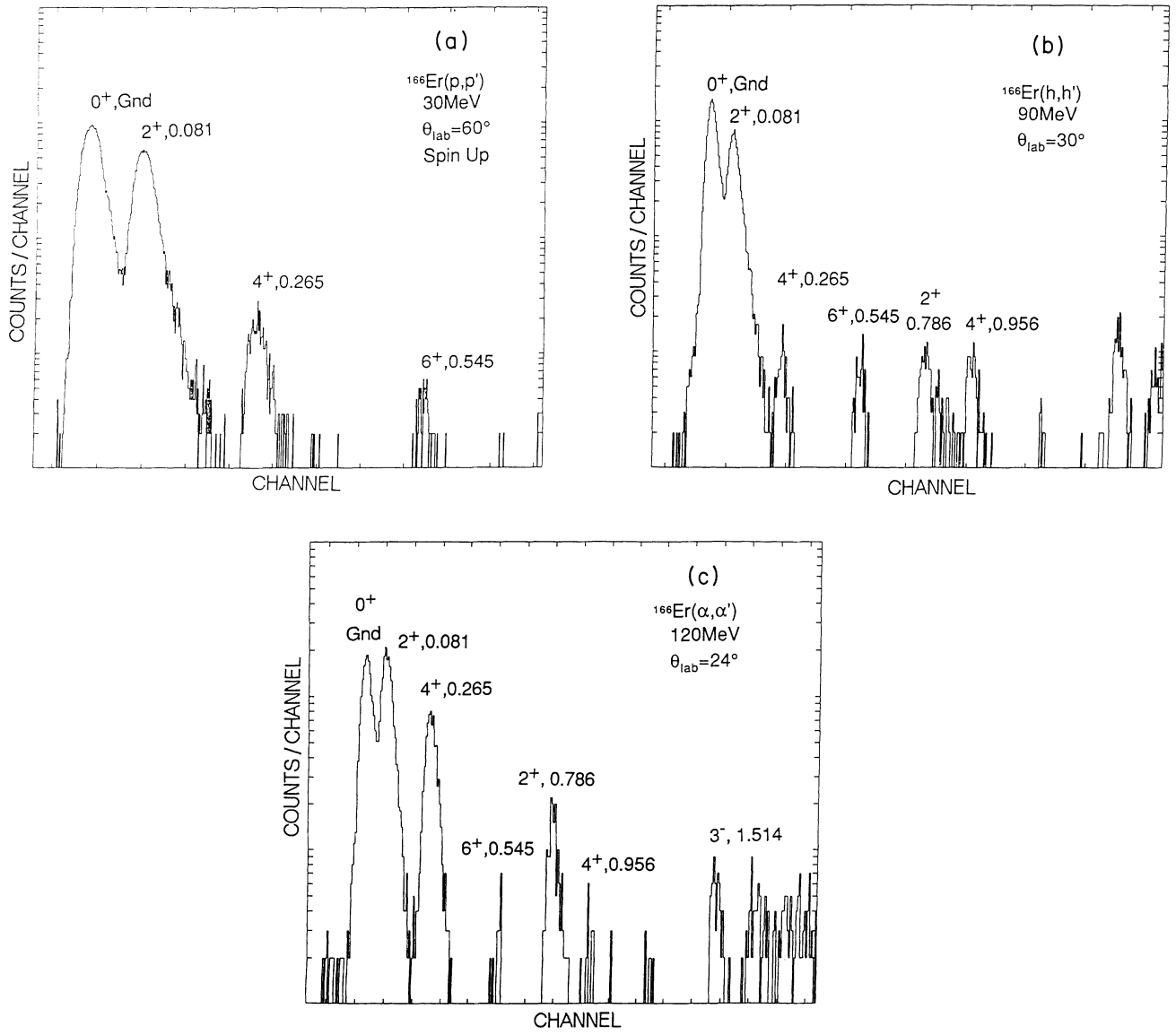

FIG. 1. Typical position spectra of the focal plane counter. (a) ^{166}Er(p,p') at $\theta_{lab}=60°$. The overall energy resolution was 13–51 keV. (b) ^{166}Er(^{3}He,^{3}He') at $\theta_{lab}=30°$. The overall energy resolution was 38–44 keV. (c) ^{166}Er(^{4}He,^{4}He') at $\theta_{lab}=24°$. The overall energy resolution was 38–59 keV.

In these analyses, 3% errors were added to the statistical uncertainties in a quadratic form as follows:

$$\delta\left[\frac{d\sigma}{d\Omega}\right]=\left[\delta\left[\frac{d\sigma}{d\Omega}\right]_{\text{stat}}^{2}+\left[\frac{d\sigma}{d\Omega}\right]^{2}\times 0.03^{2}\right]^{1/2}, \tag{4}$$

$$\delta A_y=\sqrt{[\delta A_y]_{\text{stat}}^{2}+0.03^{2}}\ . \tag{5}$$

These errors are required to include unknown systematic errors and to prevent the χ^2 search from being trapped in unphysical local minimums. In addition to the potential parameters described below, the common normalization factors of the cross sections were searched for.

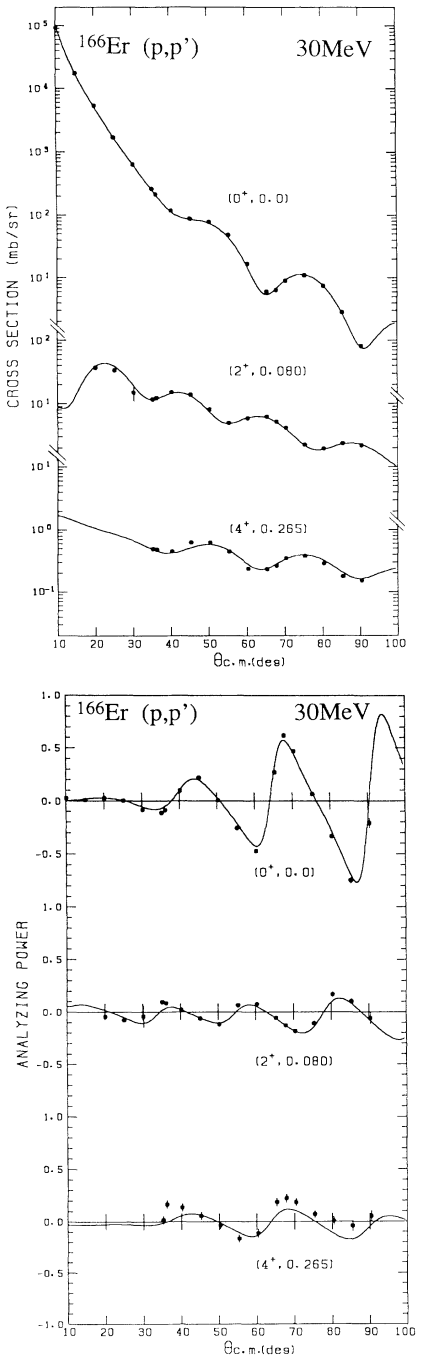

FIG. 2. Measured cross sections and analyzing powers for the ^{166}Er(p,p') reaction at 30 MeV. The error bars on the experimental data represent the statistical uncertainties. The solid curves are the best-fit result of the coupled-channels analyses based on the symmetric rotational model. The DOP parameters are listed in Table I.

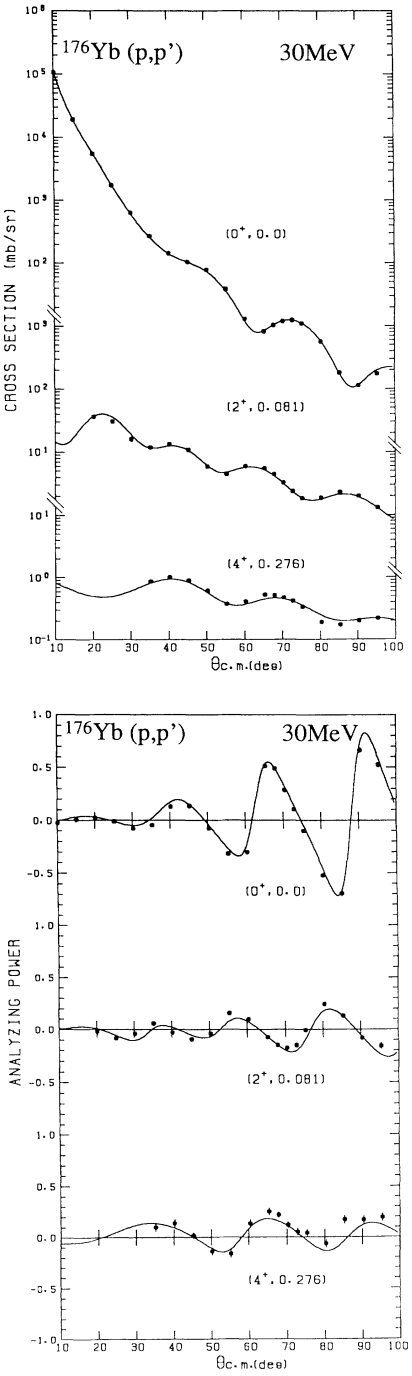

FIG. 3. Same as Fig. 2 except for ^{176}Yb.

A. Proton scattering

The DOP is written as follows:

$$U_{\mathrm{DOP}}(r,\theta)= V_{\mathrm{Coul}}(r;r_C(\theta),a_C)-V_R f(r;r_R(\theta),a_R)-iW_{wv}f(r;r_{wv}(\theta),a_{wv}) +4ia_{ws}W_{ws}\frac{d}{dr}f(r;r_{ws}(\theta),a_{ws})+V_{ls}\left[\frac{\hbar}{m_\pi c}\right]^2\frac{1}{r}\frac{d}{dr}f(r;r_{ls}(\theta),a_{ls})\sigma\cdot l \ , \tag{6}$$

where f is the Woods-Saxon form factor:

$$f(r;r_j(\theta),a_j)=(1+\exp\{[r-r_j(\theta)A^{1/3}]/a_j\})^{-1} \ . \tag{7}$$

The deformed radius $r_j(\theta)$ is expressed in the following form by using the symmetric rotational model:

$$r_j(\theta)=r_j^0\left[1+\sum_{\lambda=2,4,6}\beta_\lambda{}^j Y_{\lambda 0}(\theta)\right] , \tag{8}$$

where the suffix j represents each part of the potential; the Coulomb part (Coul), the real part (R), the volume imaginary part (wv), the surface imaginary part (ws), and the spin-orbit part (ls). The 0^+, 2^+, and 4^+ levels of the ground-state rotational band have been included in the fitting procedure. All the geometrical parameters (V,r_j^0,a_j) and the deformation parameters (β_λ^j) except for the Coulomb part were searched for.

For the search of the deformation parameters, we adopted the moment scaling procedure used in our previous work [1–3]. In this procedure, the deformation parameters of the real part were searched for, and the deformation parameters of the other parts except for the Coulomb part were adjusted so that the form factor of the other parts may have the same multipole moments as the real part. The deformation parameters of the Coulomb part were adjusted so that the multipole moments of the Fermi distribution are equal to those of the charge distribution.

B. ^{4}He scattering

The analysis was made with the following DOP:

$$U_{\mathrm{DOP}}(r,\theta)= V_{\mathrm{Coul}}(r;r_C(\theta),a_C)-V_R f(r;r_R(\theta),a_R) -iW_{wv}f(r;r_{wv}(\theta),a_{wv}) +4ia_{ws}W_{ws}\frac{d}{dr}f(r;r_{ws}(\theta),a_{ws}) \ . \tag{9}$$

The elastic- and the inelastic-scattering data for the 0^+, 2^+, 4^+, and 6^+ states of the ground-state rotational band have been included in the fitting procedure. All the geometrical parameters except for the Coulomb part were searched for. The deformation parameters of each potential part were independently searched for because the moment scaling procedure described above did not fit the data well. For the Coulomb part, the same deformed

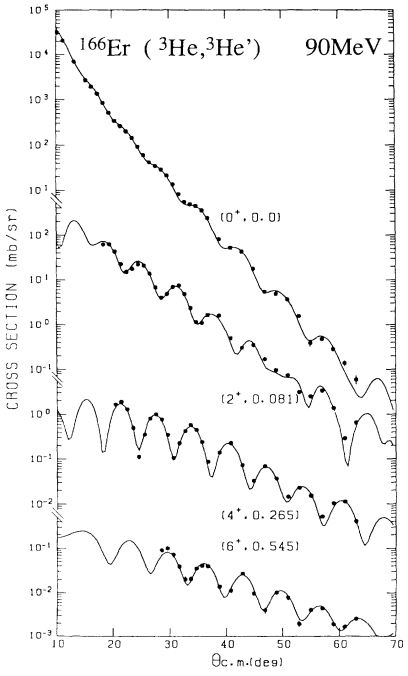

FIG. 4. Measured cross sections for the ^{166}Er(^{3}He,^{3}He′) reaction at 90 MeV. The solid curves are the best-fit result of the coupled-channels analyses based on the symmetric rotational model.

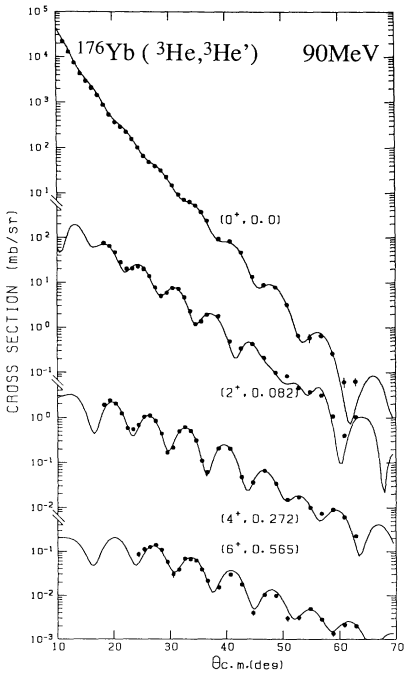

FIG. 5. Same as Fig. 4 except for ^{176}Yb.

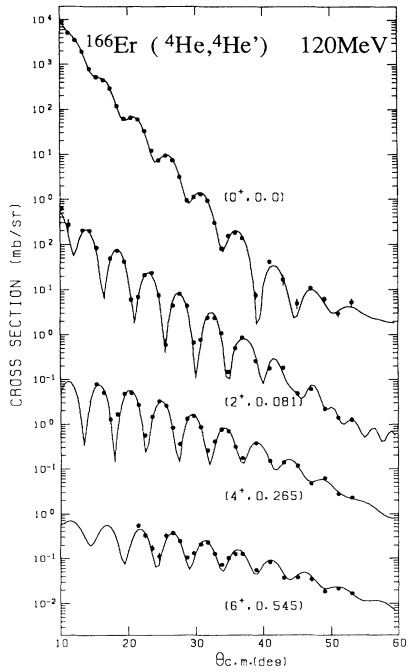

FIG. 6. Measured cross sections for the ^{166}Er(^{4}He,^{4}He') reaction at 120 MeV. The solid curves are the best-fit result of the coupled-channels analyses based on the symmetric rotational model.

radius and the diffuseness were used as those employed in the analysis of the proton scattering.

C. ^{3}He scattering

Since the ^{3}He particle has spin of $\frac{1}{2}$, the optical potential should have a spin-orbit part. This experiment was, however, performed with the unpolarized beam. At the 30-MeV/nucleon region, no experiment has been performed using the polarized ^{3}He beam, and the spin-orbit part has not yet been determined. Furthermore, the form factors of the spin-orbit part derived from the microscopic calculations [19] are quite different from the conventional form determined from the 33-MeV experiments [20]. Since both of them explain the data equally well, there would be ambiguities in the form factor of the spin-orbit part. Therefore, in this work, the data were fitted using the potential without the spin-orbit part. The DOP's are written in the same form as Eq. (9). The elastic- and the inelastic-scattering data for the 0^+, 2^+, 4^+, and 6^+ states of the ground-state rotational band have been included in the fitting procedure. The potential parameters were searched for in the same way employed in the analysis of the ^{4}He scattering. Fitting to the data has also been tried including a spin-orbit part whose form factor was set to be almost the same as those obtained from the ^{208}Pb(^{3}He,^{3}He) reaction at 33 MeV [20]. The differences between the Q_2 moments of the real parts of DOP's obtained from this analysis and those obtained from the analysis without the spin-orbit part were about 1%. The spin-orbit part is, thus, considered to play a minor on the Q_2 moments of the real part.

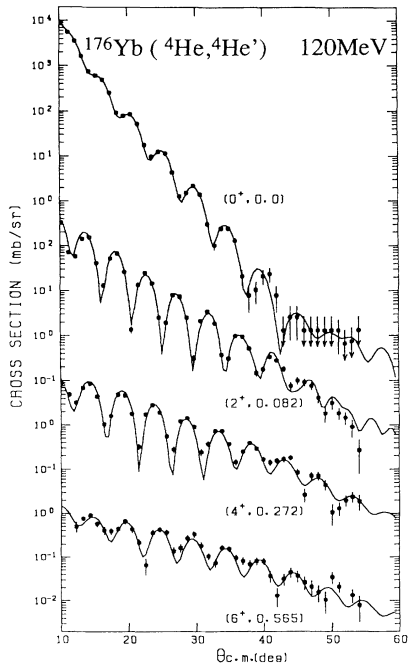

FIG. 7. Same as Fig. 6 except for ^{176}Yb.

The solid curves in Figs. 2–7 show the best-fit calculations to the data. The DOP parameters are listed in Table I. Very good fits have been obtained as shown in the figures.

IV. DISCUSSIONS

In this section, nuclear reaction mechanisms reflected in the quadrupole (Q_2) moments of the DOP's are discussed.

First, the Q_2 moments of the DOP's are calculated and they are compared with those of the charge distributions. These comparisons provide us a criterion for the folding model description of the DOP's (Sec. IV A).

Secondly, the Q_2 moments of the real parts of the DOP's and those of the folded potentials are compared. The folding model calculation is performed using a density-dependent effective interaction based on the nuclear matter calculation (Sec. IV B).

Finally, the dynamical effects of inelastic and rearrangement channels to the Q_2 moments of the real parts of the DOP's are studied. The DOP's obtained in Sec. III have been determined by taking into account only the rotational excitations. Thus, the real parts of the DOP's contain the dynamical effects of the reaction channels other than the rotational excitations. These effects are basically caused through the processes schematically shown in Fig. 9, exciting a higher-energy state [for example, the level "GDR" in Fig. 9(a)], and then coming back to the ground-state rotational band. They are more or less reflected in the Q_2 moments of the DOP's. Particularly, the processes finally going to the 2^+ state are the most effective for the Q_2 moments since the transition strength to the 2^+ state is expressed in terms of the Q_2 moments.

The reaction channels that may have dynamical effects

TABLE I. Best-fit DOP parameters. These parameters are obtained from the best-fit searches in the coupled-channels calculations for the members of the ground-state rotational band. The Coulomb potential is that of the deformed Fermi distribution as $r_c = 1.11$ fm and $a_c = 0.58$ fm and its multipole moments are set to be equal to the charge multipole moments.

Reaction	V_R	r_R	a_R	W_v	r_{wv}	a_{wv}	W_s	r_{ws}	a_{ws}	V_{ls}	r_{ls}	a_{ls}	χ^2/N[a]
p-^{166}Er[b]	50.857	1.208	0.6542	3.167	1.090	0.6999	8.024	1.227	0.6750	5.552	1.170	0.5735	2.68
p-^{176}Yb[b]	51.819	1.202	0.6567	2.572	1.107	0.7421	8.594	1.198	0.7107	6.495	1.179	0.6066	3.12
^{3}He-^{166}Er[c]	129.355	1.143	0.8725	4.223	1.386	0.3563	22.417	1.258	0.8077				3.43
^{3}He-^{176}Yb[c]	130.035	1.142	0.8503	3.064	1.456	0.9780	24.112	1.216	0.8105				3.32
^{4}He-^{166}Er[c]	131.472	1.262	0.7232	2.112	1.702	0.5113	42.228	1.257	0.5317				1.86
^{4}He-^{176}Yb[c]	130.978	1.260	0.7517	2.873	1.581	0.7100	36.725	1.249	0.5988				2.56

Reaction	β_2^R	β_4^R	β_6^R	β_2^{wv}	β_4^{wv}	β_6^{wv}	β_2^{ws}	β_4^{ws}	β_6^{ws}	β_2^{ls}	β_4^{ls}	β_6^{ls}	Renorm.
p-^{166}Er[b]	0.2776	0.0083	−0.0154	0.3257	0.0121	−0.0217	0.2693	0.0074	−0.0138	0.2971	0.0114	−0.0202	0.97
p-^{176}Yb[b]	0.2648	−0.0526	−0.0119	0.3005	−0.0628	−0.0139	0.2632	−0.0513	−0.0107	0.2681	−0.0607	−0.0164	0.96
^{3}He-^{166}Er[c]	0.2835	0.0095	−0.0062	0.2070	0.0886	−0.0530	0.2544	0.0031	−0.0121				0.95
^{3}He-^{176}Yb[c]	0.2679	−0.0345	−0.0133	0.1371	−0.0155	−0.0016	0.2822	−0.0553	0.0016				0.94
^{4}He-^{166}Er[c]	0.2635	0.0113	−0.0080	0.1955	−0.0091	−0.0021	0.2657	−0.0020	−0.0181				0.99
^{4}He-^{176}Yb[c]	0.2473	−0.0376	−0.0003	0.1957	−0.1147	0.0046	0.2600	−0.0693	−0.0182				0.96

[a]χ^2 per data point.
[b]Deformation parameters were searched for so that the multipole moments of each form factor of the optical potential were equal except for the Coulomb potential.
[c]Deformation parameters were searched for independently except for the Coulomb potential.

on the DOP's are the following ones; vibrational excitations, giant resonances, pickup channels, and breakup channels for the composite projectiles. These effects are not treated in the present folding model. Since the effective interaction is based on the nuclear matter calculation, some aspects of the nuclear finiteness are neglected. For example, the folded potentials do not include the dynamical contribution coming from the vibrational excitations which is closely related to the nuclear finiteness. Furthermore, two-nucleon correlations in nuclei are obscured in the localized form of the effective interaction, and the contributions from the rearrangement channels and the breakup channels are not taken into account in the folding model.

Therefore, the estimation and the elimination of the dynamical effects in the optical potentials should be made in comparing the Q_2 moments of the DOP's with those of the folded potentials. These effects can be estimated by the explicit coupled-channels analyses including the related channels. In Sec. IV C, the contribution from giant resonances is estimated for the 30-MeV proton scattering. In Sec. IV D, the effect of neutron pickup channels is studied for the proton scattering and also the effect of the breakup channels, which is expected to be the most significant for the composite projectiles, is discussed through the Q_2 moments of the DOP's.

The contributions from the other reaction channels can be neglected. For example, the contribution from the vibrational excitations is considered to be small because even the γ vibration, which is most easily excited among the vibrational modes, has been shown to give a negligibly small contribution to the Q_2 moments [21]. Furthermore, the transfer reactions of more than two nucleons have smaller cross sections than one-nucleon transfer reactions, and they can be also neglected.

A. Quadrupole moments of the DOP

The Q_2 moments of the real and the imaginary part of a DOP are defined, respectively, as follows:

$$Q_2^{\mathrm{R}}(U_{\mathrm{DOP}})=Ze\frac{\int f(r;r_R(\theta),a_R)r^2Y_{20}(\theta)d\mathbf{r}}{\int f(r;r_R(\theta),a_R)d\mathbf{r}} \tag{10}$$

and

$$Q_2^{\mathrm{Im}}(U_{\mathrm{DOP}})=Ze\frac{\int [W_v f(r;r_{wv}(\theta),a_{wv})-4a_{ws}W_s(d/dr)f(r;r_{ws}(\theta),a_{ws})]r^2Y_{20}(\theta)d\mathbf{r}}{\int [W_v f(r;r_{wv}(\theta),a_{wv})-4a_{ws}W_s(d/dr)f(r;r_{ws}(\theta),a_{ws})]d\mathbf{r}}, \tag{11}$$

where Ze is the electric charge of the target nucleus. These multipole moments are related to those of the matter distributions by means of the folding model [4,22], and they are favorable for the microscopic study of the nuclear reaction mechanisms, as pointed out in Sec. I.

In this work, the multipole moments of the point nucleon density are assumed to be equal to those of the charge distributions determined by the electron scattering [23] in the same manner as our previous work [1–3,8]. This assumption is assured by the analysis of the proton inelastic scattering from ^{154}Sm and ^{176}Yb at 800 MeV [7], which suggests that the multipole moments of the proton and neutron distributions are almost equal to each other.

The values of the Q_2 moments obtained from the present work are compared with those from other experiments in Fig. 8 and Table II. The uncertainties of the Q_2 moments of the real parts, shown by bars in Fig. 8, are defined as the values where the total χ^2 values of the coupled-channels analyses reach the value larger than their minimum by 10%. These "10% uncertainties" are not the statistical ones calculated using the error matrices of the χ^2 fitting, but represent the sensitivities of the Q_2 moments to the fitting. Although the error matrices provide quite small uncertainties for $Q_2^{\mathrm{R}}(U_{\mathrm{DOP}})$'s (about 0.2% of their values), the estimation using the error matrices is not suitable in the present case where strong correlations exist between the potential parameters. Therefore, we have adopted the "10% uncertainties" to represent the accuracy of the Q_2 moments. Since the common normalization factors are applied in getting the optical potential parameters from the elastic- and inelastic-scattering data, the multipole moments are insensitive to the normalization factor. For example, the

TABLE II. Multipole moments of the imaginary part of DOP's.

Nucleus	Reaction	(MeV)	Q_2 (e b)	Q_4 (e b^2)	References
^{166}Er	(p,p')	30	2.91	0.43	This work
	(d,d')	56	2.72	−0.31	S. Hirata [8]
	(^{3}He,^{3}He')	90	2.84	0.29	This work
	(^{4}He,^{4}He')	120	3.05	0.30	This work
^{176}Yb	(p,p')	30	2.78	−0.21	This work
	(d,d')	56	2.95	−0.72	S. Hirata [8]
	(^{3}He,^{3}He')	90	2.99	−0.18	This work
	(^{4}He,^{4}He')	120	3.00	−0.60	This work

Q_2^R's vary within half of the "10% uncertainties" even when the normalization factors are changed from their optimum values by ±5%.

As shown in Fig. 8, the Q_2 moments of the real parts for the ^{4}He particles at 120 MeV are larger than those of the charge distributions [$Q_2(\rho_{ch})$'s] by about 5%. We will show that these values are well explained by the folding model calculation based on a density-dependent interaction. The $Q_2^R(U_{DOP})$'s for the 50-MeV ^{4}He particles are also quite larger than the $Q_2(\rho_{ch})$'s [24]. On the other hand, the $Q_2^R(U_{DOP})$'s for the 30-MeV protons are almost the same as the $Q_2(\rho_{ch})$'s. The $Q_2^R(U_{DOP})$ for the 35-MeV proton scattering from ^{176}Yb [25] is also nearly equal to the $Q_2(\rho_{ch})$. The Q_2 moments for the ^{3}He particles at 90 MeV are slightly smaller than the $Q_2(\rho_{ch})$'s and nearly equal to those for the 56-MeV deuterons [8].

The Q_2 moments of the imaginary parts are considerably larger than those of the charge distributions. This is due to the surface imaginary part, which is large in this energy region [26].

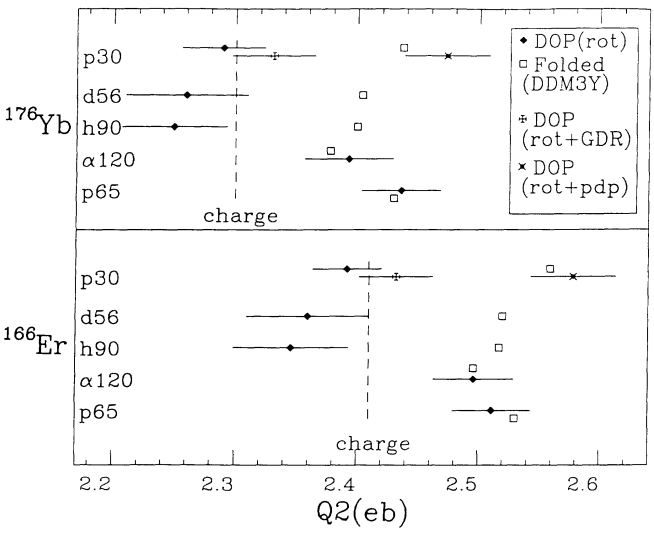

FIG. 8. Quadrupole moments of the real part of the DOP's (Q_2^R) obtained by the analyses based on the symmetric rotational model (closed diamonds) and those of the folded potentials based on the DDM3Y interaction (open boxes). The vertical axis represents the projectiles: 30-MeV protons (p30), 56-MeV deuterons (d56), 90-MeV ^{3}He particles (h90), 120-MeV ^{4}He particles (α120), and 65-MeV protons (p65). For the 30-MeV protons, the Q_2 moments obtained from the coupled-channels analyses including the GDR state (rot+GDR) and those from the analyses including the deuteron channels (rot+pdp) are also shown. The error bars are defined so that the total χ^2 values of the fit reach values larger than the minimum by 10%. The statistical errors calculated by the error matrices are quite small; for example, 0.005 for the Q_2 moments for the 30-MeV protons. The values for the 65-MeV protons (p65) and the 56-MeV deuterons (d56) are taken from Refs. [1] and [8], respectively. The dashed lines represent the values of the charge Q_2 moments [23]. Some symbols are shifted vertically to be seen clearly.

B. Folding model calculation

A single folded potential U_{SF} comparable with the DOP for the (p,p') reaction and a double folded potential U_{DF} comparable with the DOP's for the (^{4}He,^{4}He') and the (^{3}He,^{3}He') reactions are written as follows, respectively:

$$U_{SF}(\mathbf{r})=\int \rho_A(\mathbf{r}_1)v_{eff}(|\mathbf{r}-\mathbf{r}_1|,\rho)d\mathbf{r}_1 \tag{12}$$

and

$$U_{DF}(\mathbf{r})=\int\int \rho_a(\mathbf{r}_1)\rho_A(\mathbf{r}_2) \times v_{eff}(|\mathbf{r}+\mathbf{r}_1-\mathbf{r}_2|,\rho)d\mathbf{r}_1 d\mathbf{r}_2 , \tag{13}$$

where ρ_a and ρ_A are the point nucleon distributions of a projectile and a target nucleus, respectively.

In this work, the density-dependent M3Y [5] interaction has been used for v_{eff}. This interaction has the following form:

$$v_{eff}(r,\rho)=t_0(r)F(\rho) , \tag{14}$$

where t_0 is written as follows in MeV units:

$$t_0(r)=\left[7999\frac{e^{-4r}}{4r}-2134\frac{e^{-2.5r}}{2.5r}\right] -276\left[1-0.005\frac{E}{A}\right]\delta(r) . \tag{15}$$

E/A in Eq. (15) is the incident energy (in MeV) per nucleon. The density-dependent factor $F(\rho)$ is given by

$$F(\rho)=C[1+\alpha\exp(-\beta\rho)] . \tag{16}$$

The parameters C, α, and β are dependent on energy and they are calculated to fit the density dependence of Brueckner-Hartree-Fock calculations for the nuclear matter [27]. The results are $C=0.313$, $\alpha=3.325$, and $\beta=8.871$ at 30 MeV/nucleon. $F(\rho)$ is a decreasing function of the density ρ. This tendency is due to the Pauli-blocking effect which reduces the strength of the nucleon-nucleon interaction when the density of nucleons is high. The Q_2 moments of the folded potentials based on the effective interaction become, consequently, larger than those of the matter distributions, as will be shown later.

One of the possible prescriptions of the density ρ in Eq. (16) is that ρ is the density midway between the two interacting nucleons. Thus, we assumed in the folding integral of Eq. (12) that $\rho=\rho_A[(\mathbf{r}+\mathbf{r}_1)/2]$. In Eq. (13), we used a more convenient form of $\rho=\rho_a(\mathbf{r}_1)+\rho_A(\mathbf{r}_2)$ instead of

$$\rho=\rho_a[(\mathbf{r}_1+\mathbf{r}_2)/2]+\rho_A[(\mathbf{r}_1+\mathbf{r}_2)/2] .$$

This substitution gives only slight changes in the Q_2 moments because M3Y is a short-range interaction.

ρ_A is assumed to have the deformed Woods-Saxon shape. Its parameters were derived [1] from the charge density and they are listed in Table III. ρ_a is taken as a Gaussian form

TABLE III. Matter distributions.

	^{166}Er[a]	^{176}Yb[a]	^{3}He	^{4}He
R_m	6.090	6.334		
a_m	0.470	0.470		
β_2^m	0.3334	0.3073		
β_4^m	0.0171	−0.0537		
β_6^m	−0.0148	−0.0080		
Q_2 (e b)	2.41	2.30		
Q_4 (e b^2)	0.294	−0.013		
Q_6 (e b^3)	0.010	−0.054		
ρ_a^0			0.2081	0.4229
r_a			1.373	1.193

[a]These are point proton distributions of deformed Fermi forms derived from the charge densities obtained by the electron-scattering data assuming that the diffuseness a_m is 0.47 fm.

$$\rho_a(\mathbf{r})=\rho_a^0 \exp\left[-\frac{r^2}{r_a^2}\right], \tag{17}$$

where r_a and ρ_a^0 have been adjusted to reproduce the matter mean-square radius and the mass number of the projectile [28,29]. Their values are also listed in Table III.

The results of the folding calculations are summarized in Table IV and compared in Fig. 8 with the experimental values. As shown in Fig. 8, the Q_2 moments of the DOP's obtained from the ^{4}He scattering data are very well reproduced by the folding model calculation. The hexadecapole (Q_4) moments are also in good agreement with the folding model. On the other hand, the folding model calculations overestimate the $Q_2^{\mathrm{R}}(U_{\mathrm{DOP}})$'s for the 30-MeV proton scattering and those for the ^{3}He scattering by about 6%. These discrepancies suggest the presence of some characteristic reaction mechanisms that are not included in the effective interaction or the folded potentials. We will explain these discrepancies in the following subsections.

C. Effect of giant dipole resonance

Among various giant resonance modes, the giant dipole resonance (GDR) has been chosen for the study for the following reasons: (1) The GDR is excited through small-l transfer ($\Delta l=1$). (2) Since the transition strength of the isoscalar giant resonances is smaller than those of the low-lying vibrational modes, the contributions from the isoscalar resonances cannot exceed those from the γ vibrations which have been already found to give a negligibly small effect on the Q_2 moments [21]. (3) Considering the good agreement between the Q_2 moments of the DOP's for ^{4}He particles and those of the folded potentials, there seemed to be some effects of isovector excitations causing the discrepancy of the Q_2 moments for the 30-MeV protons.

The GDR in axially symmetric deformed nuclei splits into two modes (the $K=0$ mode and the $K=1$ mode). In this work, a single doorway state of the $K=0$ mode, which corresponds to the oscillation along the symmetric axis at the excitation energy of $\varepsilon=80/A^{1/3}$ MeV, has

TABLE IV. Results of folding calculations.

Target	Projectile		Q_2 (e b)	Q_4 (e b^2)
^{166}Er	p	Expt.[a]	2.392(28)	0.270(39)
		Folded[b]	2.559	0.330
	^{3}He	Expt.[a]	2.344(40)	0.291(55)
		Folded[b]	2.517	0.322
	^{4}He	Expt.[a]	2.496(33)	0.336(45)
		Folded[b]	2.494	0.316
^{176}Yb	p	Expt.[a]	2.290(34)	−0.104(32)
		Folded[b]	2.437	−0.032
	^{3}He	Expt.[a]	2.250(40)	−0.087(50)
		Folded[b]	2.400	−0.025
	^{4}He	Expt.[a]	2.393(36)	−0.033(42)
		Folded[b]	2.378	−0.022

[a]Multipole moments of the real part of the DOP's derived from the present experiment. The symmetric rotational model has been assumed (the conventional analyses).
[b]Multipole moments of the folded potentials using the DDM3Y interaction.

been taken into account, in which the transition strength of this state was made to exhaust all the $E1$ energy-weighted sum rule.

The coupling scheme used in the present calculation is shown in Fig. 9(a). The transition matrix elements for the GDR have been calculated on the assumption that the transition potential to the GDR is expressed in terms of a deformed symmetry potential. This assumption is a simple extension of the model proposed for the inelastic excitations of the GDR by protons in spherical nuclei [30]. The coupling matrix element between the levels of the ground-state rotational band are expressed in terms of the DOP's. These matrix elements were put into ECIS88 as external form factors. The integrated cross sections to the GDR states are about 2.2 mb. A brief description of the calculation is given in Appendix A. It has been confirmed that the calculated cross section to the GDR in the ^{208}Pb(p,p') reaction at 61 MeV [30] is reproduced in the similar manner using ECIS88.

Fitting to the experimental data for the ground-state rotational band has been performed with the coupled-channels calculation including the inelastic channel to the GDR. The DOP parameters have been searched for using the moment scaling procedure described in Sec. III. Table V shows the best-fit parameters. The Q_2 moments of the real part of the DOP's are illustrated in Fig. 8. As shown in the figure, the values of the Q_2 moments rise up and the discrepancies between the Q_2 moments of the folded potentials and those of the DOP's are reduced by about 20%.

D. Effects of neutron pickup channels and breakup channels

The processes via the intermediate deuteron channels [(p,d,p) process] are expected to have a significant con-

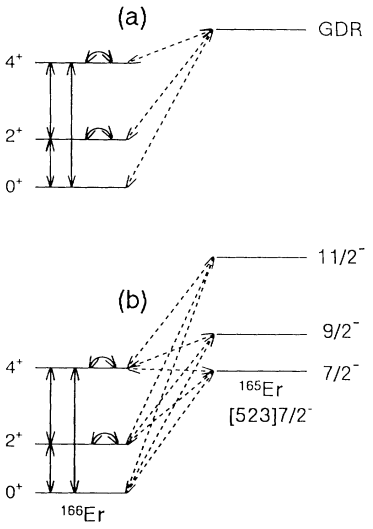

FIG. 9. (a) The coupling scheme used in the calculation including the GDR state, and (b) the deuteron channels. The coupling to the $[523]\frac{7}{2}^-$ band is shown as an example for the latter case. The transition form factors between the rotational levels (solid lines) are expressed in terms of the deformed optical potential. The coupling matrix elements indicated by the dashed lines are given in the appendices.

TABLE V. Best-fit DOP parameters obtained from the best-fit searches in the coupled-channels calculation including the GDR and the deuteron channels for the 30-MeV protons. The Coulomb potential is that of the deformed Fermi distribution as $r_c = 1.11$ fm and $a_c = 0.58$ fm and its multipole moments are set equal to the charge multipole moments. Deformation parameters were searched for so that the multipole moments of each form factor of the optical potential were equal except for the Coulomb potential.

Reaction	V_R	r_R	a_R	W_v	r_{wv}	a_{wv}	W_s	r_{ws}	a_{ws}	V_{ls}	r_{ls}	a_{ls}	χ^2/N^a
p-^{166}Er[b]	49.755	1.224	0.6233	3.471	1.427	0.7372	6.359	1.198	0.5685	5.482	1.171	0.5793	3.10
p-^{176}Yb[b]	49.571	1.230	0.6185	2.921	1.337	0.7241	7.364	1.165	0.6864	6.043	1.170	0.6396	3.22
p-^{166}Er[c]	51.879	1.206	0.6810	4.294	1.557	0.5107	7.002	1.248	0.2910	5.524	1.175	0.5346	3.78
p-^{176}Yb[c]	52.991	1.207	0.6921	3.303	1.388	0.6805	6.826	1.229	0.6290	6.331	1.204	0.5577	3.81
d[d]	120.0	1.170	0.7900	0			21.0	1.320	0.6800	6.2	1.01	0.75	

Reaction	β_2^R	β_4^R	β_6^R	β_2^{wv}	β_4^{wv}	β_6^{wv}	β_2^{ws}	β_4^{ws}	β_6^{ws}	β_2^{ls}	β_4^{ls}	β_6^{ls}	Renorm.
p-^{166}Er[b]	0.2776	0.0083	−0.0154	0.3257	0.0121	−0.0217	0.2693	0.0074	−0.0138	0.2971	0.0114	−0.0202	0.97
p-^{176}Yb[b]	0.2648	−0.0526	−0.0119	0.3005	−0.0628	−0.0139	0.2632	−0.0513	−0.0107	0.2681	−0.0607	−0.0164	0.96
p-^{166}Er[c]	0.2939	0.0186	−0.0200	0.1944	0.0077	−0.0075	0.2910	0.0251	−0.0291	0.3148	0.0258	−0.0283	0.96
p-^{176}Yb[c]	0.2793	−0.0460	−0.0170	0.2176	−0.0306	−0.0063	0.2741	−0.0453	−0.0122	0.2883	−0.0499	−0.0154	0.96

[a]χ^2 per data point.
[b]Best-fit parameters obtained from the coupled-channels analyses including the inelastic excitation of the GDR state.
[c]Best-fit parameters obtained from the coupled-channels analyses the including deuteron channels.
[d]Deuteron potential parameters used for the coupled-channels calculations.

tribution to the proton scattering when the incident energy is comparable to the energy of the Fermi motion. There are some calculations for 30-MeV protons predicting that the polarization potentials arising from the deuteron channels are repulsive and that these potentials cause considerable effects of about 10% on the volume integral of the real part of the optical potentials [31,32]. A typical coupling scheme is given in Fig. 9(b). The couplings between the rotational levels in the deuteron channels are neglected because these transitions give higher-order contributions to the proton channels. We have calculated the coupling matrix elements between the proton and deuteron channels, by applying the strong-coupling limit for the internal Hamiltonian of the residual nuclei, and by using the zero-range approximation for the calculation of the nuclear matrix elements. The transition form factors, therefore, consist of the neutron wave functions multiplied by the expansion coefficients of Nilsson orbits, the occupation probabilities, and the geometrical factors [33].

These calculations of the coupling matrix elements provide a selection rule for one-nucleon transfer reactions in the deformed nuclei. According to it, the coupling with the inelastic proton channel takes a complicated scheme consisting of various combinations of angular momentum transfer (l,j). Thus, the deuteron channels can strongly affect the Q_2 moments of the DOP's.

The exact coupled-channels calculation including the deuteron channels is only made by taking into account all the possible neutron orbits consisting of valence orbits and core ones. Since it is extremely complicated to perform the calculation strictly, a selection of the neutron orbits would be necessary. In the present calculation, only the valence orbits of the principal quantum number $N=5$ have been taken into account for the following reasons. (1) The (p,d) reactions mainly occur at the nuclear surface region where the valence nucleons are dominant. (2) The valence nucleons are correlated with the shape deformation of the nuclei, and they dominate the rotational motion. (3) The effect of the core orbits on the Q_2 moments would be negligible because the neutron pickup cross sections from the core orbits are quite small and, as shown in Appendix B, the two-step amplitudes leading to the rotational excitations via the neutron pickup channels from the closed-shell orbits vanish when they are summed up in neglecting the small differences of the reaction Q values. (4) The neutron pickup cross sections from the $N=6$ valence orbits are considerably small because most of them are originated from the $1i_{\frac{13}{2}}$ orbit in ^{166}Er and ^{176}Yb.

The one-neutron hole states of the $N=5$ Nilsson orbit amount to over 20 states in ^{165}Er and ^{176}Yb, and the exact treatment of all these states in the coupled-channels calculations is still too complicated. Instead of the exact treatment, an approximate prescription has been introduced, with which the number of the deuteron channels is reduced while the two-step amplitudes from the ground state to the members of the ground band via the deuteron channels are approximately conserved. The outline of the prescription is given in Appendix B. It also gives a good approximation to the (p,d) cross sections.

The coupled-channels calculations including the deuteron channels have been performed using ECIS88. The approximated values of the integrated (p,d) cross sections in ^{166}Er are 0.8, 3.7, 2.3, 3.0, 1.5, and 0.3 mb for $\frac{1}{2}^-$, $\frac{3}{2}^-$, $\frac{5}{2}^-$, $\frac{7}{2}^-$, $\frac{9}{2}^-$, and $\frac{11}{2}^-$ states, respectively. In ^{176}Yb, they are 2.5, 3.5, 2.7, 5.7, 2.2, and 0.4 mb, respectively.

Fitting to the experimental data has been performed using the coupled-channels calculation including the deuteron channels. The DOP parameters have been searched for in the same way as that for taking into account the GDR. The data have been well fitted and one of the results is shown in Fig. 10. The DOP parameters are listed in Table V and the Q_2 moments of the real parts are given in Fig. 8. As shown in the figure, the coupled-channels analyses including the deuteron channels are found to provide almost the same values of the Q_2 moments as those of the folded potentials.

The calculations in which the deuteron channels are excluded were also done, and it was found that the 2^+ cross sections are increased by about 10% in the calculation. One example is shown by the dashed curves in Fig. 10. This implies the presence of the destructive interferences between the direct transition amplitude to the 2^+ state and the indirect ones via the deuteron channels. The discrepancies of the Q_2 moments of the folded potentials and those of the DOP's obtained from the conventional analyses can be attributed to these destructive interferences.

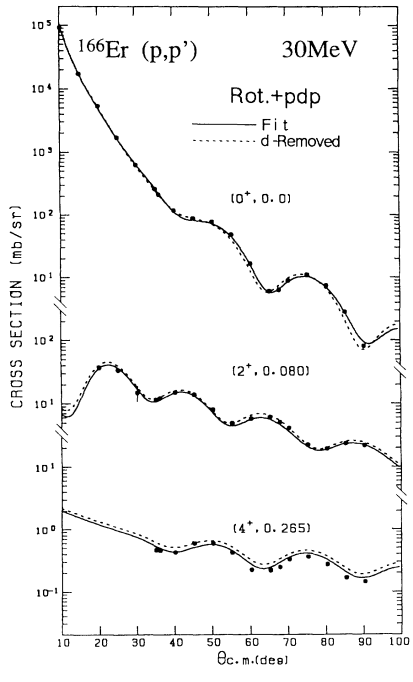

FIG. 10. One of the results of the explicit coupled-channels analyses including the deuteron channels at $E_p=30$ MeV. The solid curves represent the best-fit calculation. When the deuteron channels are excluded from the best-fit calculation, the 2^+ cross sections are increased by about 10% (the dashed curve). This result implies the presence of the destructive interferences between the direct transition amplitude to the 2^+ state and the indirect ones via the deuteron channels.

Comparisons of the experimental results of the composite projectiles (^{3}He particles, ^{4}He particles, and deuterons) among themselves suggest that the small Q_2 moments of the DOP's for deuterons and ^{3}He particles are due to the effect of the breakup channels. In general, the projectile-breakup reactions have large cross sections for the weakly bound particles; they amount to about one-third of the total reaction cross sections in the deuteron scattering, for example.

According to the CDCC (continuum-discretized coupled-channels) calculations developed recently, the breakup channels give a significant contribution to the elastic and the inelastic scattering of the composite particles having small binding energies [10]. The calculations performed for the collective excitations are particularly interesting: The cross sections for the vibrational 2^+ state in the ^{58}Ni(d,d') reactions are reduced when the breakup channels are included [10]. This result also implies the presence of the destructive interferences between the direct transition amplitude to the 2^+ state and the indirect ones via the breakup channels, in accordance with our results of the (p,d,p) contribution. Since the transition form factor to the rotational 2^+ state has a similar form to that to the vibrational 2^+ state, we can also expect that the breakup channels reduce the cross sections for the rotational 2^+ state in the deuteron scattering from deformed nuclei. Therefore, the coupled-channels calculation including the breakup channels as well as the inelastic channels are expected to reduce the discrepancies in the Q_2 moments for the deuteron and the ^{3}He scattering.

For the ^{4}He scattering, the dynamical effect coming from the breakup channels on the real part of the optical potentials is expected to be small because of the large binding energies of the ^{4}He particles. The dynamical effect is, from the viewpoint of the perturbation, the second-order contribution of the transition potential to the breakup channels. Therefore, the effect strongly depends on the reaction Q values and those from the reactions requiring large Q values are expected to be small. This would be a reason for the good agreement between the folding model calculations and the results obtained from the conventional analyses considering only the rotational excitations for the ^{4}He scattering.

V. SUMMARY AND CONCLUSIONS

Elastic and inelastic scattering of polarized protons, ^{3}He particles, and ^{4}He particles leading to the ground-state rotational band of ^{166}Er and ^{176}Yb has been measured with the incident energy of 30 MeV/nucleon, using the high-resolution spectrograph RAIDEN. Fitting to the data has been performed by the coupled-channels analyses assuming the symmetric rotational model, and the deformed optical potentials have been obtained. We have studied the nuclear reaction mechanisms through the quadrupole (Q_2) moments of the DOP's.

The Q_2 moments of the real part of the DOP's for the ^{4}He scattering were found to be larger than those of the charge distributions by about 5%. They are well explained by the folding model calculation based on the DDM3Y interaction.

The Q_2 moments for the 30-MeV protons were found to be almost equal to those of the charge distributions. For the ^{3}He scattering, the Q_2 moments are found to be smaller than those of the charge distributions. The folding model calculation, which describes well the Q_2 moments of the DOP's for ^{4}He particles, cannot reproduce the results of the protons and the ^{3}He particles. This means that, in the actual reaction processes, there might be some dynamical processes being neglected in the folding model.

Rather complete examinations have been done for solving the discrepancies of the Q_2 moments found in the 30-MeV protons scattering, and the effect of the deuteron channels (neutron pickup channels) was found to have a significant contribution to the Q_2 moments. The explicit coupled-channels calculations including the deuteron channels have been found to give almost the same values of the Q_2 moments of the DOP's as those of the folded potentials. These results imply the presence of the destructive interferences between the direct transition amplitude to the 2^+ state and the indirect ones via the deuteron channels.

Comparisons of the experimental results obtained from the experiments of the composite projectiles (d, ^{3}He, and ^{4}He) among themselves suggest that the small Q_2 moments of the DOP's for deuterons and ^{3}He particles can be attributed to the effect of the breakup channels of the incident particles. An explicit coupled-channels calculation including the breakup channels is expected to explain the discrepancies between the Q_2 moments obtained from the conventional analyses and those of the folded potentials for the ^{3}He particles and the deuterons.

ACKNOWLEDGMENTS

The authors are grateful to the staff of the cyclotron at RCNP for their cooperation during the experiment. Sincere thanks are due to M. Iwaki, Y. Sakemi, H. Kaneko, and F. Hiei of Kyoto University for their cooperation during the experiment and for many helpful discussions. The coupled-channels calculations have been done with FACOM M380-R at RCNP and FACOM M340 at Department of Physics, Kyoto University. This experiment was performed at RNCP under Program Nos. 25A19 and 27A13 and was supported in part by a Grant-in-Aid for Scientific Research No. 63044073 of Japan Ministry of Science, Culture and Education.

APPENDIX A: COUPLING TO THE GDR

In this work, the GDR is assumed to be an isovector oscillation of the rigid proton and the neutron densities against one another. Its wave function is given in Ref. [34], for example.

The model proposed for the inelastic excitations of the GDR by protons in spherical nuclei [30] has been extended to those in deformed nuclei. In the spin-orbit representation, the coupling matrix elements to the $K=0$ mode of the GDR are given by

$$\langle [(L_\beta s)J_b, I_B]J|\Delta U|[(L_\gamma s)J_c, I_C]J\rangle = \left[\frac{A\hbar^2}{NZm\varepsilon}\right]^{1/2} \sum_\lambda \tilde{v}_\lambda(r)\hat{I}_C\langle \lambda I_C 00|I_B 0\rangle \times (4\pi)^{-1/2} i^{L_\beta+L_\gamma}(-)^{J-s+\lambda+I_B+L_\beta}\hat{L}_\beta\hat{L}_\gamma\hat{J}_b\hat{J}_c \times \begin{Bmatrix} J_b & \lambda & J_c \\ I_C & J & I_B \end{Bmatrix} \begin{Bmatrix} L_\beta & L_\gamma & \lambda \\ J_c & J_b & s \end{Bmatrix} \langle L_\gamma L_\beta 00|\lambda 0\rangle , \quad \text{(A1)}$$

where I_B $(=1)$ is the spin of the GDR state and I_C $(=0,2,4,\ldots)$ is that of the rotational state of the ground band, and m is nucleon mass and $\hat{I}=\sqrt{2I+1}$. The transition form factor $\tilde{v}_\lambda$ is expressed in terms of a linear combination of the multipole v_λ of the derivative of the deformed symmetry potential,

$$\tilde{v}_\lambda(r)=\sqrt{3}\sum_{\lambda'}\left[\frac{3(2\lambda'+1)}{4\pi(2\lambda+1)}\right]^{1/2}|\langle \lambda' 100|\lambda 0\rangle|^2 v_{\lambda'}(r) , \quad \text{(A2)}$$

with

$$v_\lambda(r)=\frac{4NZ}{A^2}(\tfrac{1}{3}\pi)^{1/2}\int d\Omega\, Y_{\lambda 0}(\theta)\frac{\partial U_1}{\partial r}(r,\theta) . \quad \text{(A3)}$$

The factor $\sqrt{3}$ in Eq. (A2) has been introduced so that only the $K=0$ mode may exhaust all the $E1$ energy-weighted sum rule.

The deformed symmetry potential U_1 has been assumed to be the following:

$$U_1(r,\theta)=-Vf(r;r_V(\theta),a_V)+4ia_W W\frac{df}{dr}(r;r_W(\theta),a_W) , \quad \text{(A4)}$$

where the deformed Woods-Saxon form factor $f(r;r_j(\theta),a_j)$ and the deformed radius $r_j(\theta)$ are expressed in the same form as Eqs. (7) and (8), respectively. We used the same parameters as those in Ref. [30]: $V=10$ MeV, $W=15.5$ MeV, $r_V^0=1.16$ fm, $a_V=0.75$ fm, $r_W^0=1.37$ fm, and $a_W=[0.74-0.008E_p+(N-Z)/A]$ fm. The deformation parameters, β_λ^j, were adjusted so that each form factor may have the same multipole moments as those of the matter distributions.

APPENDIX B: COUPLING TO DEUTERON CHANNELS

The coupling matrix elements between the proton and deuteron channels are given in the following form by applying the strong-coupling limit for the Hamiltonian of the deformed nuclei, and by using the zero-range approximation for the calculation of the nuclear matrix elements [35]:

$$\langle [(L_p s_p)J_p, I_B]J|H-E|[(L_d s_d)J_d, I_C]J\rangle = \sum_{L_n s_n J_n}\delta(r_\beta-\lambda r_\gamma)\frac{1}{\lambda^2}\hat{L}_n\hat{s}_n f_{L_n s_n J_n}(r_\gamma) \times i^{L_p+L_d+L_n}(-)^{J_n+J+J_d+I_B+L_n}\frac{\hat{L}_p\hat{L}_d\hat{J}_n\hat{J}_p\hat{J}_d}{(4\pi)^{1/2}} \times \begin{Bmatrix} J_p & J_n & J_d \\ I_C & J & I_B \end{Bmatrix} \begin{Bmatrix} L_p & L_d & L_n \\ s_p & s_d & s_n \\ J_p & J_d & J_n \end{Bmatrix} \langle L_d L_p 00|L_n 0\rangle , \quad \text{(B1)}$$

where s_p (s_d), L_p (L_d) are the spin and the angular momentum of the proton (deuteron), respectively, and I_B (I_C) is the spin of the residual nuclei in the proton (deuteron) channel. λ $[=(C+1)/C]$ is the ratio of the mass number of the residual nuclei and f_{lsj} is the radial transition form factor.

The radial transition form factor can be written in the following form when the residual nucleus in the deuteron channel belongs to the rotational band of K^π [33]:

$$f_{L_n s_n J_n}(r)=\frac{\hat{I}_B\hat{s}_d}{\hat{s}_n\hat{L}_n}(-)^{s_d-s_p+s_n}D_0\sqrt{2}(-)^{2(J_n+K)}\langle I_B J_n 0,-K|I_C,-K\rangle \pi_\nu V_{\nu K\pi}C^{\nu K}_{NL_nJ_n}u_{NL_nJ_n}(r) , \quad \text{(B2)}$$

where π_ν and $V_{\nu K\pi}$ are the parity and the occupation probability of the Nilsson orbit, respectively, and $C^{\nu K}_{Nlj}$ is the expansion coefficient of the Nilsson orbit. D_0 is given by the overlap integral of the projectile wave functions.

The expansion coefficients $C^{\nu K}_{Nlj}$'s have been given by Chi [36] and the values at the deformation $\delta=0.3$ have been used. D_0 was set to be 122.5 MeV. For simplicity, the rigid Fermi surface has been assumed. The neutron orbits are filled up to the $[523]\frac{5}{2}^-$ orbit in ^{166}Er and up to $[514]\frac{7}{2}^-$ orbit in ^{176}Yb. We have calculated the neutron

wave functions in the real Woods-Saxon potentials using the separation energy method [37]. The geometrical parameters of the potentials are $r_0=1.2$ fm and $a=0.65$ fm, that are commonly used for analyses of (p,d) reactions [38,39]. The deuteron potential parameters listed in Table V are calculated based on the adiabatic model [40,41] in which we assume that the potential parameters of the neutrons are equal to those of the protons [41,32]. The global parameters given by Bechetti and Greenlees [42] have been used for the adiabatic model calculation.

For the estimation of the (p,d,p) contribution in deformed nuclei with a coupled-channels calculation, one of the most serious problems would be that the exact calculation requires quite a large number of the deuteron channels. Since the exact calculation is extremely complicated, we have taken into account only the neutron pickup channels from the $N=5$ valence orbits, and introduced a prescription with which the number of the deuteron channels is reduced while the two-step amplitudes via the deuteron channels are kept approximately unchanged, as described below.

From Eq. (B2), the two-step amplitude from the ground state to the I^+ state of the ground band via the neuron pickup channel from the Nilsson orbit νK is given by the following form:

$$T^{\nu K}_{0\to I}=|\pi_\nu|^2 V^2_{\nu K} C^{\nu K}_{Nlj} C^{\nu K}_{Nl'j'} \hat{I}\langle Ij'0,-K|j,-K\rangle G \ , \quad \text{(B3)}$$

where j is the nuclear spin in the deuteron channel and G is a factor expressed in terms of the transition form factor and the deuteron propagator. G depends on νK only through the Q value of the (p,d) reaction. Therefore, the coupled-channels calculations can be greatly simplified if (1) the separated deuteron channels with the same nuclear spin parity are "unified" to a single deuteron channel having a mean Q value and, (2) the transition form factor between these "unified" channels with the nuclear spin j and the proton channel with the nuclear spin I_B is given by the following form:

$$f^{I_B,j}_{L_n s_n J_n}(r)=\frac{\hat{s}_d}{\hat{s}_n \hat{L}_n}(-)^{s_d-s_p+s_n} D_0 \sqrt{2}\,\tilde{C}^{I_B,j}_{NL_nJ_n} u_{NL_nJ_n}(r) \ , \quad \text{(B4)}$$

under the condition that the coefficients $\tilde{C}^{I_B,j}_{Nlj}$'s satisfy the following relation:

$$\tilde{C}^{0,j}_{NL_nJ_n}\tilde{C}^{I_B,j}_{NL_n'J_n'} = \sum_{\nu K;N=5} V^2_{\nu K} C^{\nu K}_{NL_nJ_n} C^{\nu K}_{NL_n'J_n'} \hat{I}_B \langle I_B J_n' 0,-K|j,-K\rangle \ . \quad \text{(B5)}$$

Comparison of Eq. (B3) with (B5) shows that the sum of the amplitude $T^{\nu K}_{0\to I}$ is conserved approximately in the calculation based on the prescription described above. When $I_B=0$, Eq. (B5) means that the (p,d) cross sections are also approximately conserved.

In addition, we can show that the two-step amplitudes leading to the rotational excitations via the neutron pickup channels from the closed-shell orbits vanish when they are summed up in neglecting the small differences of the Q values of the (p,d) reaction. From the orthogonality of the expansion coefficient, the two-step amplitudes satisfy the following relation when G is replaced by $\bar{G}$ which is independent of νK:

$$\sum_{\nu:\text{closed}} T^{\nu K}_{0\to I}=\bar{G}\,\hat{I}\langle Ij'0,-K|j,-K\rangle \left[\sum_\nu C^{\nu K}_{Nlj} C^{\nu K}_{Nl'j'}\right] = \bar{G}\,\hat{I}\langle Ij'0,-K|j,-K\rangle \delta_{jj'}\delta_{ll'} \ , \quad \text{(B6)}$$

where the summation is taken over the orbits belonging to a closed shell (core orbits). Furthermore, with the help of the property of the Clebsch-Gordan coefficient,

$$\sum_{K=1/2,\ldots,j}\ \sum_{\nu:\text{closed}} T^{\nu K}_{0\to I}=\bar{G}\,\hat{I}\left[\sum_{K=1/2,\ldots,j}\langle Ij0,-K|j,-K\rangle\right] =0 \quad \text{for } I=2,4,6,\ldots, \quad \text{(B7)}$$

which means that the summation of the two-step amplitudes vanishes under the condition mentioned above.

[1] T. Ichihara, H. Sakaguchi, M. Nakamura, T. Noro, F. Ohtani, H. Sakamoto, H. Ogawa, M. Yosoi, M. Ieiri, N. Isshiki, Y. Takeuchi, and S. Kobayashi, Phys. Rev. C **29**, 1228 (1984).

[2] Y. Takeuchi, H. Sakaguchi, M. Nakamura, T. Ichihara, M. Yosoi, M. Ieiri, and S. Kobayashi, Phys. Rev. C **34**, 493 (1986).

[3] H. Ogawa, H. Sakaguchi, M. Nakamura, T. Noro, H. Sakamoto, T. Ichihara, M. Yosoi, M. Ieiri, N. Isshiki, and S. Kobayashi, Phys. Rev. C **33**, 834 (1986).

[4] G. R. Satchler, J. Math. Phys. **13**, 1118 (1972).

[5] A. M. Kobos, B. A. Brown, P. E. Hodgson, G. R. Satchler, and A. Budzanowski, Nucl. Phys. **A384**, 65 (1982).

[6] N. Yamaguchi, S. Nagata, and T. Matsuda, Prog. Theor. Phys. **70**, 456 (1983).

[7] M. L. Barlett, J. A. McGill, L. Ray, M. M. Barlett, G. W. Hoffmann, N. M. Hintz, G. S. Kyle, M. A. Franey, and G. Blanpied, Phys. Rev. C **22**, 1168 (1980).

[8] S. Hirata, Ph.D. thesis, Kyoto University, 1990.

[9] K. Hatanaka, K. Imai, S. Kobayashi, T. Matsusue, M. Nakamura, K. Nishimura, T. Noro, H. Sakamoto, H. Shimizu, and J. Shirai, Nucl. Phys. **A340**, 93 (1983).

[10] M. Yahiro, Y. Sakuragi, and M. Kamimura, Prog. Theor. Phys. Suppl. **89**, 32 (1986).

[11] H. Ikegami, S. Morinobu, I. Katayama, M. Fujiwara, and S. Yamabe, Nucl. Instrum. Methods **175**, 335 (1980).

[12] K. Imai, N. Tamura, and K. Nishimura, Research Center for Nuclear Physics report, 1976, p. 23.

[13] T. Ichihara, H. Sakaguchi, K. Hatanaka, M. Fujiwara, and K. Hosono, Research Center for Nuclear Physics report, 1981, p. 194.

[14] Y. Fujita, K. Nagayama, M. Fujiwara, S. Morinobu, T. Yamazaki, and H. Ikegami, Nucl. Instrum. Methods **196**,

249 (1982).
[15] I. Katayama and H. Ogata, Nucl. Instrum. Methods **174**, 295 (1980).
[16] R. Dittman, H. S. Sandau, R. K. Cole, and C. N. Waddel, Nucl. Phys. **A126**, 592 (1969); H. S. Sandau, J. M. Cameron, and W. F. McGill, *ibid.* **A169**, 600 (1971).
[17] T. Tamura, Rev. Mod. Phys. **31**, 679 (1965).
[18] J. Raynal, computer code ECIS79, Saclay (unpublished); J. Raynal, computer code ECIS88, Saclay (unpublished).
[19] T. Wada, Y. Takahashi, and H. Horiuchi, Prog. Theor. Phys. **75**, 619 (1986).
[20] Y.-W. Lui, O. Karban, S. Roman, J. M. Nelson, and E. C. Pollaco, Nucl. Phys. **A333**, 205 (1980); A. Farooq, J. D. Brown, G. Ray, and S. Roman, J. Phys. Soc. Jpn. Suppl. **55**, 752 (1986).
[21] T. Ichihara, H. Sakaguchi, M. Nakamura, M. Yosoi, M. Ieiri, Y. Takeuchi, H. Togawa, T. Tsutsumi, and S. Kobayashi, Phys. Rev. C **36**, 1754 (1987).
[22] R. S. Mackintosh, Nucl. Phys. **A226**, 379 (1976).
[23] C. W. Creswell, Ph.D. thesis, MIT, 1979.
[24] D. L. Hendrie, N. K. Glendenning, B. G. Harvey, O. N. Jarvis, H. H. Duhm, J. Saudinos, and J. Mahoney, Phys. Lett. **26B**, 127 (1968); N. K. Glendenning, D. L. Hendrie, and O. N. Jarvis, *ibid.* **26B**, 131 (1968).
[25] C. H. King, J. E. Fink, G. M. Crawley, J. A. Nolen, Jr., and R. M. Ronningen, Phys. Rev. C **20**, 2084 (1979).
[26] F. A. Brieva and B. Z. Georgiev, Nucl. Phys. **A308**, 27 (1978).
[27] J.-P. Jeukenne, A. Lejeune, and C. Mahaux, Phys. Rev. C **16**, 80 (1977).
[28] G. R. Satchler and W. G. Love, Phys. Rep. **55**, 183 (1979).
[29] T. Cooper, W. Bertozzi, J. Heisenberg, S. Kowalski, W. Turchinetz, C. Williamson, L. Cardman, S. Fivozinsky, J. Lightbody, Jr., and S. Penner, Phys. Rev. C **13**, 1083 (1976).
[30] G. R. Satchler, Nucl. Phys. **A195**, 1 (1972).
[31] R. S. Mackintosh and A. M. Kobos, Phys. Lett. B **213**, 127 (1976).
[32] P. W. Coulter and G. R. Satchler, Nucl. Phys. **A293**, 269 (1977).
[33] R. J. Ascuitto, C. H. King, L. J. McVay, and B. Sorensen, Nucl. Phys. **A226**, 454 (1974).
[34] J. M. Eisenberg and W. Gleiner, *Nuclear Theory* (North-Holland, Amsterdam, 1978), Vol. 1, p. 345.
[35] G. R. Satchler, *Direct Nuclear Reactions* (Oxford University Press, New York, 1983), Chap. 6.
[36] B. E. Chi, Nucl. Phys. **83**, 97 (1966).
[37] This procedure has been performed using a standard routine of ECIS88.
[38] Y. Toba, K. Nagano, Y. Aoki, S. Kunori, and K. Yagi, Nucl. Phys. **A359**, 76 (1981).
[39] Y. Aoki, H. Iida, K. Nagano, Y. Toba, and K. Yagi, Nucl. Phys. **A393**, 52 (1983); K. Yagi, S. Kunori, Y. Aoki, K. Nagano, and Y. Toba, Phys. Rev. Lett. **43**, 1087 (1979).
[40] J. D. Harvey and R. C. Johnson, Phys. Rev. C **3**, 636 (1971).
[41] G. R. Satchler, Phys. Rev. C **4**, 1485 (1971).
[42] F. D. Bechetti and G. W. Greenlees, Phys. Rev. **182**, 1190 (1969).